RADIATION PRESSURE AND MASS EJECTION IN #-LIKE STATES OF GRS 1915+105

Citation: Neilsen, Joseph, Ronald A. Remillard, and Julia C. Lee. "RADIATION PRESSURE AND MASS EJECTION IN ρ-LIKE STATES OF GRS 1915+105." The Astrophysical Journal 750, no. 1 (April 17, 2012): 71. © 2012 The American Astronomical Society

As Published: http://dx.doi.org/10.1088/0004-637x/750/1/71

Publisher: IOP Publishing

Persistent URL: http://hdl.handle.net/1721.1/95454

Version: Final published version: final published article, as it appeared in a journal, conference proceedings, or other formally published context

The Astrophysical Journal, 750:71 (9pp), 2012 May 1 doi:10.1088/0004-637X/750/1/71

RADIATION PRESSURE AND MASS EJECTION IN ρ-LIKE STATES OF GRS 1915+105

Joseph Neilsen[1,2,3], Ronald A. Remillard[1], and Julia C. Lee[2,3]
[1] MIT Kavli Institute for Astrophysics and Space Research, Cambridge, MA 02139, USA; jneilsen@space.mit.edu
[2] Astronomy Department, Harvard University, Cambridge, MA 02138, USA
[3] Harvard-Smithsonian Center for Astrophysics, Cambridge, MA 02138, USA
Received 2011 October 29; accepted 2012 February 29; published 2012 April 17

ABSTRACT

We present a unifying scenario to address the physical origin of the diversity of X-ray light curves within the ρ variability class of the microquasar GRS 1915+105. This "heartbeat" state is characterized by a bright flare that recurs every ∼50–100 s, but the profile and duration of the flares vary significantly from observation to observation. Based on a comprehensive, phase-resolved study of heartbeats in the *Rossi X-ray Timing Explorer* archive, we demonstrate that very different X-ray light curves do not require origins in different accretion processes. Indeed, our detailed comparison of the phase-resolved spectra of a double-peaked oscillation and a single-peaked oscillation shows that different cycles can have basically similar X-ray spectral evolution. We argue that all heartbeat oscillations can be understood as the result of a combination of a thermal–viscous radiation pressure instability, a local Eddington limit in the disk, and a sudden, radiation-pressure-driven evaporation or ejection event in the inner accretion disk. This ejection appears to be a universal, fundamental part of the ρ state, and is largely responsible for a hard X-ray pulse seen in the light curve of all cycles. We suggest that the detailed shape of oscillations in the mass accretion rate through the disk is responsible for the phenomenological differences between different ρ-type light curves, and we discuss how future time-dependent simulations of disk instabilities may provide new insights into the role of radiation pressure in the accretion flow.

Key words: accretion, accretion disks – black hole physics – instabilities – X-rays: binaries – X-rays: individual (GRS 1915+105)

Online-only material: color figures

1. INTRODUCTION

As one of the brightest and most variable sources in the X-ray sky, the microquasar GRS 1915+105 is an excellent case study for the investigation of evolving accretion flows. Discovered in 1992 by Castro-Tirado et al. (1992), the black hole has been in outburst for over 17 years and has become famous for its superluminal jets (Mirabel & Rodríguez 1994), its bizarre X-ray variability (Belloni et al. 2000, hereafter B00; Klein-Wolt et al. 2002; Hannikainen et al. 2005), and its disk–jet interactions (Fender & Belloni 2004; Fender et al. 2004; Neilsen & Lee 2009; Neilsen et al. 2011).

Of its many classes of X-ray variability, the best studied are the χ state, which produces steady optically thick jets (see, e.g., Dhawan et al. 2000; Klein-Wolt et al. 2002), the β state, a wild 30 minute cycle with discrete ejection events (Mirabel et al. 1998), and the ρ state, which is affectionately known as the "heartbeat" state for the similarity of its light curve to an electrocardiogram (see Figure 1). The ρ-type cycle consists of a slow rise followed by a short bright pulse, repeating with a period of roughly 50 s (Taam et al. 1997; B00).

After nearly two decades of X-ray monitoring of GRS 1915+105, it is clear that its remarkable diversity of X-ray states is also reflected in the states themselves. Indeed, even in their original paper on these variability classes, B00 divide the χ class into four sub-categories that differ in hardness and noise properties. Furthermore, some observations may exhibit characteristics of multiple states (e.g., β-type variations; Neilsen et al. 2012), and various instances of a single state may even differ in their large-scale variability patterns. For example, Massaro et al. (2010, hereafter M10) recently analyzed a long *Beppo*SAX observation of GRS 1915+105 in the ρ state and reported significant changes in the light-curve shape: the number of pulses or peaks per cycle ranged from one to at least four. These pulses can be separated by 10 s or more, and the later peaks are typically harder (Taam et al. 1997; Paul et al. 1998).

In the hopes of uncovering direct evidence for the origin of these luminous ρ-type pulses, we performed the first joint *Chandra*/*RXTE* phase-resolved spectral analysis of an observation of GRS 1915+105 in the ρ state (Neilsen et al. 2011). Using the *Chandra* gratings (Canizares et al. 2005), we showed for the first time that changes in the broadband X-ray spectrum drive physical changes in the accretion disk wind on timescales as short as 5 s, and that this wind is sufficiently massive to cause state transitions in the disk. Based on *Rossi X-ray Timing Explorer* (*RXTE*) spectra, we argued that radiation pressure plays several key roles in the accretion disk, from driving the observed limit cycle via the Lightman–Eardley instability (aka radiation pressure instability, RPI; Lightman & Eardley 1974; Belloni et al. 1997; Janiuk et al. 2000) to literally pushing the inner edge of the accretion disk away from the black hole (a local Eddington limit; Fukue 2004; Heinzeller & Duschl 2007; Lin et al. 2009) until the global Eddington limit is reached and the disk is evaporated or ejected at the maximum accretion rate (see also Janiuk & Czerny 2005). For this last point, we argued that the second peak in our double-peaked light curves could be explained as bremsstrahlung emitted when the ejected gas collides with the corona.

But what is the significance of these results when some instances of the ρ state only have a single peak (M10)? That is, if there is no "second peak" in the light curve, is mass ejection still required to explain the X-ray oscillation? Are we to understand different variations of the ρ-like cycles as driven by the same physical processes or as producing similar

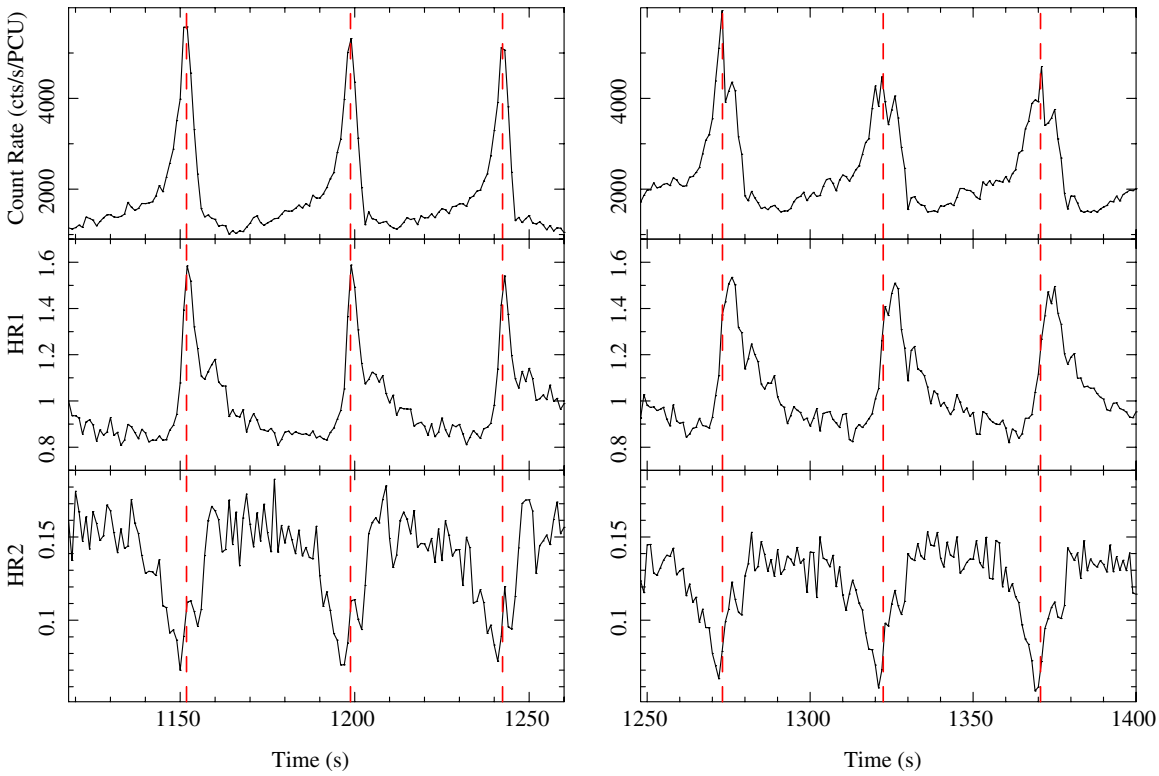

Figure 1. Sample cycles from PCA observations of single-peaked (left) and double-peaked (right) oscillations: (top) count rate light curves, (middle) HR1, and (bottom) HR2. These sample cycles are taken from observations 40703-01-07-00 and 60405-01-02-00, respectively. In this paper, we analyze all *RXTE* observations of ρ-like cycles; the data here are representative of the broad behavior. For reference, we have marked peak count rate times (identified by cross-correlation; see Section 2) with dashed vertical lines.

(A color version of this figure is available in the online journal.)

light curves by coincidence? In this paper, we begin to address the remarkable diversity *within* the variability classes of GRS 1915+105, with a comprehensive phase-resolved study of all the heartbeat-like states in the *RXTE* archive.

We describe the observations, data analysis, and phase folding in Section 2. In Section 3, we perform a detailed comparison of the timing and spectral behavior of single- and double-peaked ρ states. In Section 4, we interpret our results as clear evidence that a single physical scenario may produce a wide variety of light curves, and we consider the exact origin of the variations observed by Massaro et al. (2010).

2. OBSERVATIONS AND PHASE FOLDING

Since its launch in 1995 (Jahoda et al. 1996), *RXTE* has observed GRS 1915+105 roughly twice a week, for a total of over 1600 pointings as of the original writing of this paper. In this paper, we will focus exclusively on the data from the Proportional Counter Array (PCA), which covers approximately 2–60 keV. We extract 1 s normalized light curves from the binned data modes in three energy channels: $A \equiv 2$–5 keV, $B \equiv 5.2$–12 keV, and $C \equiv 12$–45 keV. The light curves are normalized using the PCA light curve of the Crab Nebula. That is, for each Proportional Counter Unit (PCU), we renormalize the mission-long Crab light curve to count rate values 1100, 1140, and 330 counts s^{-1} for channels A, B, and C, respectively. This roughly corresponds to the raw count rate of PCU2 around MJD 52,000. We then apply these same normalizations to the GRS 1915+105 count rates so that the intensity scale is the same for all observations. We also produce two hardness ratios: HR1 $= B/A$ and HR2 $= C/B$.

In order to identify ρ-state observations, we examined 1 s light curves and color–color diagrams (CD) for all observations of GRS 1915+105. We selected observations with regular or quasi-regular bursts of the appropriate shape, duration, and CD by visual inspection. This task can be rather tricky since there are variations within the heartbeat state (Section 1) as well as strong resemblances between the ρ class and some portions of the ν and κ classes; our analysis may include some cycles from these classes. However, the fact that our phase-folding method can be used for all these quasi-regular cycles is indicative of the physical robustness of our results. We show samples of the light curves and hardness ratios for two typical (long) observations in Figure 1 (*RXTE* observations 40703-01-02-00 and 60405-01-02-00 on the left and right, respectively). The oscillation is obvious in all panels. Inspection of these data and our ensemble of light curves reveals the same variations noted by M10, namely, that the number of strong peaks in the light curve changes over timescales of days or longer, as do the durations of the pulses and the time delays between them. As we will see later that there is likely a continuum of light-curve shapes, we will not devote any time here to detailed phenomenological categorizations of these profiles.

In Neilsen et al. (2011), we showed that we can very accurately characterize the physics of this oscillation by phase folding the individual cycles, which takes into account the variable oscillation period. In other words, we stretch or compress and then combine all the individual cycles in a given observation, and study the spectral conditions at each part of the cycle. We determine the start times of each cycle by means of an iterative cross-correlation method that is described in more detail in Neilsen et al. (2011). Briefly, we use cross-correlations to

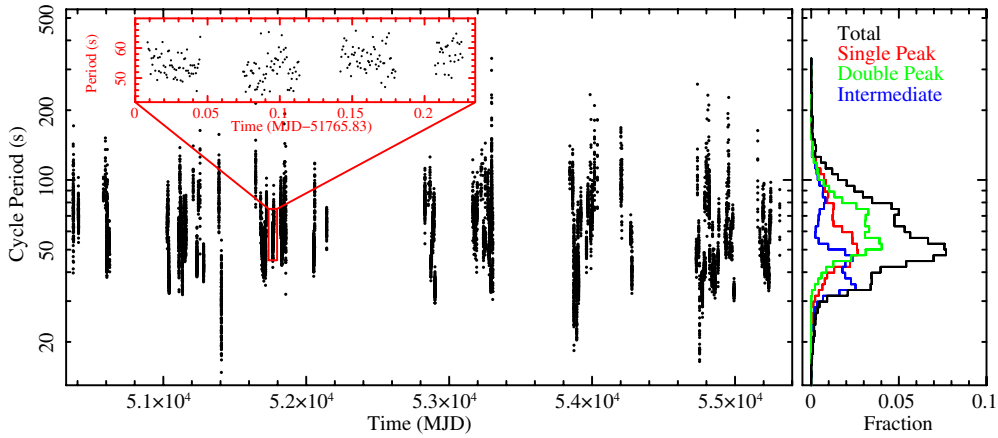

Figure 2. Left: the measured period of the ρ cycle for all the analyzed observations. Periods cluster around 50–60 s, although there are some excursions as high as 340 s. The inset shows the drift and scatter that characterize the cycle period in a typical observation. Right: the distribution of periods colored according to peak multiplicity.

(A color version of this figure is available in the online journal.)

identify the main peak in the count rate for each cycle, and then define the times of peak count rate as phase $\phi \equiv 0$. With this analysis, we measure 10,068 peak times in 242 observations. For reference, we plot the resulting cycle periods (i.e., the distance between successive times of $\phi = 0$) in Figure 2. It is evident from this figure that typical periods are $\lesssim$100 s, although some single cycles may last over 300 s. Within a given observation, there is a fair amount ($\gtrsim$10%) of cycle-to-cycle scatter in the period, but the period is usually very stable around the mean (see inset, Figure 2).

Once we have defined a phase ephemeris for all 242 observations, we create phase-folded light curves for each, and then we identify them as single-peaked, double-peaked, or as intermediate cases. Observations may be classified as intermediate if there is substantial noise (e.g., if the observation only includes a few cycles) or if the cycles have unusual shapes or strong period variability (like κ-type cycles), so that it is difficult to reliably distinguish two individual pulses from a single pulse. Of the 242 observations included here, we classify 101 as having double-peaked cycles, 77 as single-peaked, and the remaining 64 as intermediate cases. Because there is an inherent difficulty in deciding whether structure in the light curve is noise or a physical peak, there is an uncertainty in these numbers of about 10–15 (estimated by repeating the classification). This uncertainty has no effect on the subsequent spectroscopy or our physical interpretation.

There are some statistical differences in the period between cycles with different numbers of peaks. The right panel of Figure 2 shows that single- and double-peaked cycles have similar periods, at 61 $\pm$ 23 s and 64 $\pm$ 18 s, respectively, while intermediate cycles are generally shorter, with an overall mean of 52 $\pm$ 27 s. The uncertainties represent the sample standard deviations; the standard errors of the mean are $\lesssim$0.5 s. At very short periods, the intermediate cycles show a bimodal period distribution, which is reminiscent of the κ state (B00) or the irregular bursts studied by Yadav et al. (1999). However, we will see that these intermediate cases exhibit similar spectral behavior to single- and double-peaked cycle types, so they are unlikely to represent a completely different physical phenomenon.

Figure 3 shows the phase-folded light curves for the single- and double-peaked observations illustrated in Figure 1. The average phase-folded light-curve profiles, shown as solid lines, are superimposed on the individual cycles from these same observations shown as gray points. There are a total of 204 cycles and 265 cycles on the left and right, respectively. The scatter is limited and it is clear that within an observation the individual cycles have the same profile. On the other hand, it is also clear that heartbeats can differ substantially from one observation to the next (i.e., in terms of the number of peaks or pulses). Building on our prior study of double-peaked cycles (Neilsen et al. 2011), we focus in this paper on a comparison between single-peaked cycles and double-peaked cycles, and the question: can these two cycle types be produced by the same mechanism? In other words, does the single pulse correspond to the first (soft) pulse of a double-peaked cycle, the second (hard) pulse, a combination of the two pulses, or is it completely different?

3. THE SINGLE PULSE

In this section, based on timing analysis and broadband spectroscopy, we develop a case that the single pulse in single-peaked cycles corresponds to the second, hard pulse in double-peaked cycles. As such, our results will indicate that the physical processes responsible for the production of this hard pulse are active in all ρ-like cycles. In other words, these processes are fundamental to the heartbeat state.

3.1. Folded Light Curves and Timing Analysis

The first indications that the single pulse is analogous to the hard pulse come from the light curves and phase-folded light curves in Figures 1 and 3. In these plots, HR2 rises sharply from its minimum value around $\phi = 0$, giving the appearance of a local maximum. The local maximum in HR2 coincides with the maximum value of HR1 in both single-peaked and double-peaked cycles. This phase of "maximum spectral hardness" occurs during the main pulse in single-peaked cycles, while it is very close to the second pulse when there are two peaks in the cycle.

An alternative indication of this same phenomenon is the delay between various maxima in the hardness ratios and in the hard and soft X-ray light curves. For example, consider that in a double-peaked cycle, HR1 peaks at the same time as the *C*-band light curve, but after the *A* band, while all three quantities are synchronized in single-peaked observations.

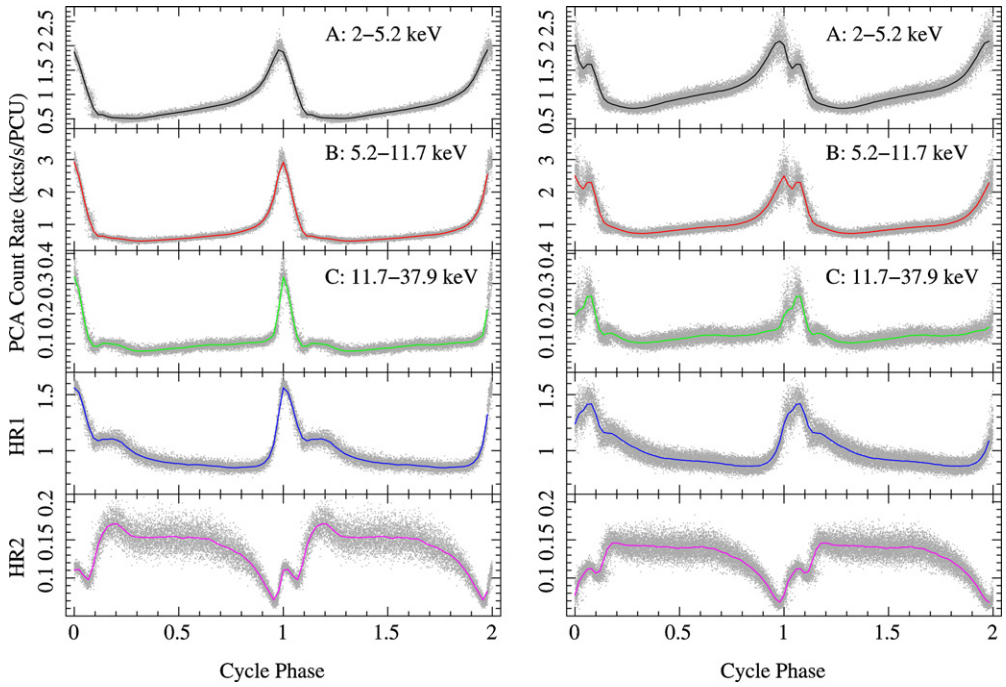

Figure 3. Average phase-folded light curves and hardness ratios for the single- and double-peaked oscillations depicted in Figure 1, i.e., *RXTE* observations 40703-01-07-00 and 60405-01-02-00, respectively. Two cycles are shown for clarity. The smooth curves represent the average light-curve profiles, and the data are plotted in gray (204 cycles on the left, 265 cycles on the right). It is obvious that despite the scatter and variations in the period, the phase profile of the ρ oscillation is remarkably constant from cycle to cycle. Note that the energy ranges plotted here differ from Neilsen et al. (2011) because we are using new, normalized light curves (Section 2).

(A color version of this figure is available in the online journal.)

The delays between these maxima are easily quantified from the phase-folded light curves, and we present the phase delay distributions in Figure 4. It should come as no surprise that double-peaked oscillations exhibit a significant delay between the hard and soft X-ray pulses (top panel): $\Delta\phi_{C-A} = 0.08 \pm 0.05$, where the uncertainty is the sample standard deviation. As the average period of these oscillations is ∼64 s, we find that the hard pulse typically follows the soft pulse by ∼4.9 s. For single-peaked cycles, the delay between the peaks in the *A* and *C* bands is much smaller (consistent with zero): $\Delta\phi_{C-A} = 0.02 \pm 0.02$. The intermediate cases show a bimodal distribution, apparently including mixed contributions from single-peaked and double-peaked cycles. As suggested above, all cycle types exhibit a very short delay between the maximum of HR1 and the hard X-ray pulse. This delay is $\Delta\phi_{\mathrm{HR1}-C} = 0.02 \pm 0.04$ for single-peaked cycles, 0.01 ± 0.04 for double-peaked cycles, and 0.01 ± 0.03 for intermediate cases.

Also relevant are the values of the hardness ratios themselves. In Figure 5, we present the distribution of HR2 at $\phi = 0$, when the count rate is at a maximum (top), and at the maximum of the *C*-band light curve (bottom). In general, we see that at $\phi = 0$, double-peaked oscillations are softer than cycles with a single peak (intermediate cases lie in between the two). This is to be expected if the single pulse corresponds to the hard pulse of a double-peaked cycle. That is, when there are two peaks, our cross-correlation method picks out the brighter, softer first pulse for $\phi = 0$; in the absence of the soft pulse (i.e., one pulse only), $\phi = 0$ coincides with the hard pulse. The bottom panel of Figure 5 confirms this conjecture: all cycles have very similar HR2 when the *C*-band flux is maximized. This suggests that a common light source produces a pulse of hard X-rays in every cycle.

Again, the relative timing of the X-ray flux and spectral hardness ratios indicates that the intermediate cases represent a continuum of profiles between single- and double-peaked oscillations. A completely different physical process might be less likely to produce the same timing signatures, so we conclude that at 1 s resolution, the variations in the cycle profile can be explained in the context of two main pulses, one soft and one hard, whose relative strengths, durations, and separations can vary from observation to observation. In Section 3.2, we employ phase-resolved spectra to unify these pulses in a single physical framework.

3.2. Phase-resolved Spectroscopy

In Neilsen et al. (2011), we showed that in a double-peaked cycle (*RXTE* ObsID 60405-01-02-00), the X-ray spectrum of the hard pulse was described very well as the sum of the two major components: a disk blackbody and a power-law-type component, possibly bremsstrahlung or Comptonized disk emission. Statistically, we could not distinguish between different Comptonization models and bremsstrahlung emission, but all models required a sudden decrease in the electron temperature associated with this component during the hard pulse.

In this section, we ask whether an observation of a single-peaked cycle can be described by the same model with similar phase dependence; we return to the physical interpretation of this model in Section 4. We perform phase-resolved spectroscopy of the single-peaked observation represented in Figures 1 and 3, *RXTE* ObsID 40703-01-07-00, and compare to our results on the double-peaked cycle in Neilsen et al. (2011). We implicitly assume that these two observations are representative of single- and double-peaked heartbeats. This assumption is justified by our results in Section 3.1, which demonstrate clear similarities between different observations of a given type of cycle.

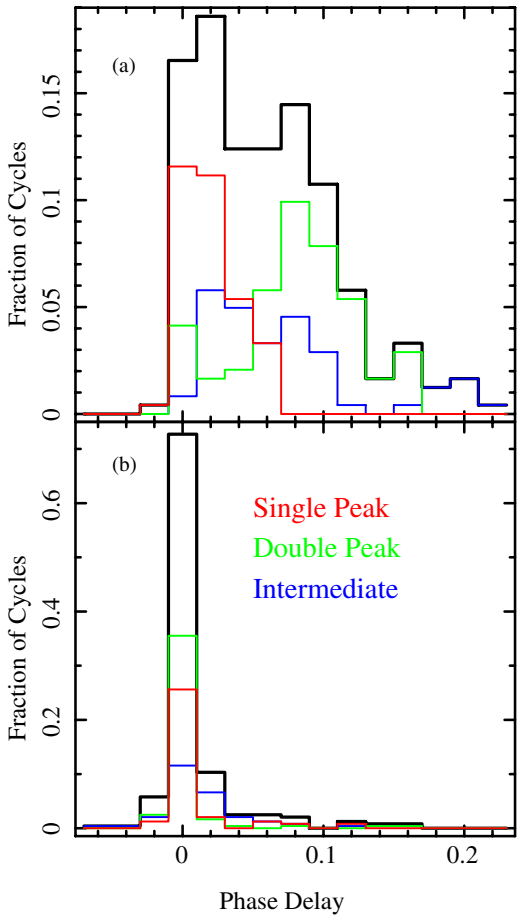

Figure 4. Distribution of phase delays between maxima in (a) the *A* and *C* bands and (b) the *C* band and HR1, for all observations analyzed in this paper. The top panel shows that single-peaked cycles generally have a small delay between their soft and hard maxima, but double-peaked oscillations have a much longer delay. In this respect, the intermediate cases sometimes mimic single-pulse profiles and sometimes behave like double-peaked cycles. The bottom panel demonstrates that there is no significant difference between any cycle types in the delay between the maximum in HR1 and the maximum in the hard X-ray light curve, although HR1 typically peaks a little later than the *C*-band light curve itself.

(A color version of this figure is available in the online journal.)

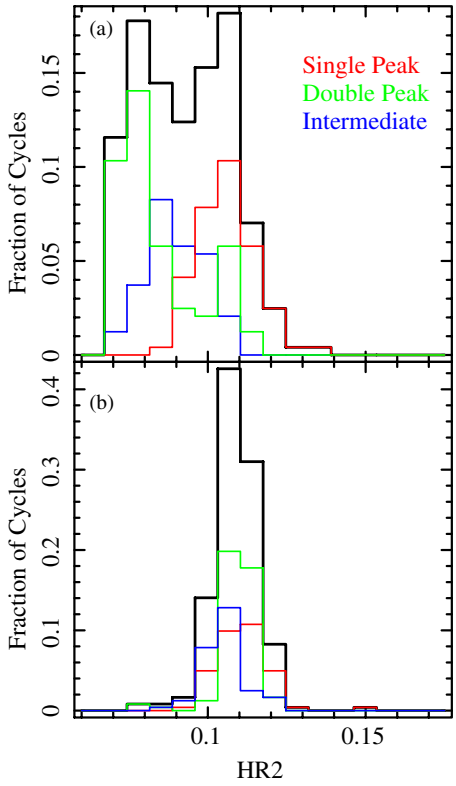

Figure 5. Distribution of HR2 at two phases of the heartbeat cycle for all observations analyzed in this paper: (top) $\phi = 0$, and (bottom) at the maximum of the *C*-band light curve. The top panel shows that double-peaked cycles are typically softer than single-peaked cycles at their respective times of $\phi = 0$, while the bottom panel shows that both types of cycle have very similar hardness near the maximum of the *C*-band light curve. Thus, the single pulse may correspond to the *hard (second)* pulse of double-peaked cycles.

(A color version of this figure is available in the online journal.)

Our spectral model consists of interstellar absorption by cold gas (`tbabs`; Wilms et al. 2000), a hot disk (`ezdiskbb`; Zimmerman et al. 2005) convolved through a scattering kernel (`simpl`; Steiner et al. 2009), a Gaussian emission line at 6.4 keV, and a high-energy cutoff (`highecut`, with functional form $\exp(-E/E_{\rm fold})$ for $E > E_{\rm cut}$; we set $E_{\rm cut} = 0$). `simpl` takes a seed spectrum and scatters a fraction $f_{\rm SC}$ of the source photons into a power law, approximating the high temperature, low optical depth regime of Comptonization. We use `highecut` to account for curvature in the hard X-ray spectrum, and we prefer `simpl` to `powerlaw` because it conserves photons and includes a physically realistic rollover at low energies. Our method is precisely the same as that reported in Neilsen et al. (2011): we extract phase-resolved spectra and responses and, applying the model described above, we fit the emission from 3 to 45 keV. All spectral fitting is done in ISIS (Houck & Denicola 2000; Houck 2002). We assume a distance and inclination of $D = 11.2$ kpc and $i = 66^\circ$ (Fender et al. 1999); we fix $N_{\rm H} = 5 \times 10^{22}$ cm^{-2} (Lee et al. 2002, and references therein). Overall, the model provides an excellent description of the data, with a reduced $\chi^2/\nu = 1847.6/2149 = 0.86$.

The resulting fit parameter values for our single-peaked oscillation are shown in black in Figure 6. The maximum observed temperature in the disk, $T_{\rm obs}$, is mostly constant near 1.1 keV throughout the cycle but spikes to ~2.2 keV at $\phi = 0$. While the disk temperature hovers around 1.1 keV, the inner disk radius $R_{\rm in}$ rises steadily from ~60 km to ~95 km, but then turns over and plummets quickly to ~40 km (we use a color-correction factor $f = 1.9$, appropriate for high luminosity; J. Steiner 2010, private communication). The `simpl` photon index Γ, the scattering fraction $f_{\rm SC}$, and the high-energy cutoff $E_{\rm fold}$ all decrease steadily for most of the cycle, from roughly 4 to 1.5, 0.9 to 0.1, and $\gtrsim$500 keV to 30 keV, respectively. Near $\phi = 0$, Γ and $f_{\rm SC}$ rise sharply, but $E_{\rm fold}$ (i.e., the electron temperature) dips to 5 keV. During this brief dip, there is also weak evidence of a coincident dip in Γ.

For comparison, we overplot our (Neilsen et al. 2011) measured parameters for the double-peaked oscillation. Given the differences in the light curves (Figure 1), the similarity of the spectral fits is striking. The most important difference is a clear phase shift: a given feature in a given parameter occurs later in phase in double-peaked cycles. In terms of the parameters themselves, the double-peaked cycle has a slightly higher and flatter baseline in $T_{\rm obs}$, and the spike is smaller; the disk radius increases for a longer interval relative to the single-peaked cycle. The double-peaked cycle also has a slightly larger photon index, scattering fraction, and electron temperature than the single-peaked oscillation.

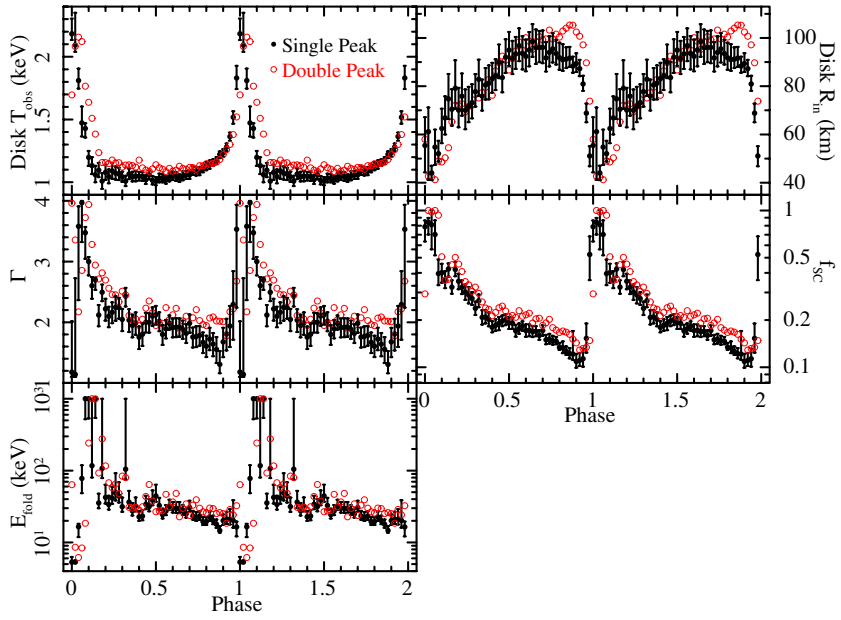

Figure 6. Model-fit parameters and their 90% confidence limits as a function of phase for the PCA spectra of the single-peaked heartbeat oscillation (filled black points; *RXTE* observation 40703-01-07-00). For comparison, we overplot our parameters for a double-peaked cycle (open red circles; Neilsen et al. 2011, *RXTE* observation 60405-01-02-00). Two cycles are shown for clarity. Since the oscillation periods are near 50 s, each phase bin corresponds to roughly 1 s of real time. The fits are extremely similar; in conjunction with the phase shift between the two parameter sets, this result implies that the pulse in single-peaked cycles physically corresponds to the hard second pulse in double-peaked cycles.

(A color version of this figure is available in the online journal.)

Two points from our spectral fits deserve special consideration.

1. It is remarkable that in these two very different cycles, the measured radius of the disk plummets sharply and comes to rest (albeit briefly) at the same value of $R_{\rm in} \sim 40$ km. The possibility of a "touchdown" radius is especially interesting given that 40 km is the radius where one expects the peak emission from a thin disk around a maximally spinning 14 $M_{\odot}$ black hole (McClintock et al. 2006).
2. Both single-peaked and double-peaked oscillations are marked by a short interval where the scattering fraction approaches one and $E_{\rm fold}$ drops to ∼5 keV, indicating the sudden appearance of an optically thick population of relatively cool electrons. In double-peaked cycles, this interval corresponds to the hard pulse. In single-peaked cycles, it coincides with the main peak in the light curve at $\phi = 0$. This connection confirms the identification of the single pulse as the hard pulse.

On the whole, it is abundantly clear that the same spectral processes are operating in both of these cycles.

4. DISCUSSION

In Section 3, our phase-resolved timing and spectral analysis demonstrated that single-peaked heartbeats should be interpreted as double-peaked cycles with a weak soft pulse, while the brief pulse of hard X-rays is truly fundamental to the ρ cycle. In this section, we consider the origin of these pulses and the implications of their relative variations.

In our detailed phase-resolved spectral analysis of a double-peaked oscillation (Neilsen et al. 2011), we explored two Comptonization models (`simpl` and `nthcomp`; Zdziarski et al. 1996; Życki et al. 1999) and also bremsstrahlung as descriptors of the broadband X-ray emission in the heartbeat state. While these models differ in their physical interpretations, they implied very similar behavior in the inner accretion disk, and all three models required the sudden appearance of a new population of electrons with a temperature of ∼5 keV during the hard pulse. We argued that this was probably due to the sudden ejection of matter from the disk at very high luminosity (see Janiuk & Czerny 2005 for a theoretical basis).

To produce the waves in $\dot{M}$ that cause the system to exhibit these changes on a cyclic basis, we invoked a global Eddington instability (Lightman & Eardley 1974; Neilsen et al. 2011). This instability, a class of thermal–viscous instability (Taam et al. 1997; Nayakshin et al. 2000), has also been called the RPI (Janiuk et al. 2000; Janiuk & Czerny 2005), a term we adopt in what follows. We also found a long interval of increasing disk radius at constant temperature, which we argued was an indication of a local Eddington limit in the disk (Fukue 2004; Heinzeller & Duschl 2007; Lin et al. 2009). Local Eddington effects can occur in geometrically thin disks when the local vertical component of radiation pressure becomes sufficiently strong to overcome gravity, disrupting the disk interior to some critical radius. In short, when the RPI raises the local accretion rate, the disk responds via the local Eddington process: it maintains a constant temperature but increases its inner radius as it expels a ring of gas at $R_{\rm in}$ (Fukue 2004; Heinzeller & Duschl 2007; Lin et al. 2009). These phenomena (mass ejection and the local Eddington process) reflect the critical importance of radiation pressure in the accretion dynamics of double-peaked heartbeat states.

Furthermore, in the single-peaked cycle we have studied here, the same two effects (i.e., mass ejection and disk evolution via a local Eddington limit) also dominate the spectral evolution. Thus, we believe that a single unified model can successfully describe the various light curves of ρ-like states, and we identify radiation pressure as the driver of this unified model. From the oscillating mass accretion rate (the RPI) to the slow growth of the disk radius (the response of a luminous thin

disk to the rising accretion rate) to the ejection or evaporation of the inner disk (a consequence of the sudden final influx of matter), radiation pressure mediates all major aspects of the ρ cycle.

If a common set of accretion processes can describe the range of ρ-like cycles seen in the *RXTE* archive, then we must also address the question: why are some oscillations different than others? If the hard pulse is always observed in the heartbeat state, then where does the soft pulse go? To answer this important question, we look to the comparison of our spectral parameters in Figure 6. The salient features of the phase evolution of the disk are the plunge of $R_{\rm in}$ toward the black hole and the rapid heating of the inner disk. Ultimately, it is the timing of this plunge relative to the spike in the disk temperature that determines the cycle profile and the relative strengths of the two pulses.

But examining the evolution of $R_{\rm in}$ and $T_{\rm obs}$ in light of the role of radiation pressure in the heartbeat state, we see two puzzles that merit further consideration. First, why are the changes in the disk so catastrophic? In principle, the local Eddington process is reversible, so that $R_{\rm in}$ could also *decrease* slowly at roughly constant temperature (e.g., reversible changes tied to the local Eddington limit appear to operate along the flaring branch of Z sources; Lin et al. 2009). But in the heartbeat state of GRS 1915+105, the symmetry appears to be broken: the disk expands and contracts along vastly different paths in the $R_{\rm in} - T_{\rm obs}$ plane. It is unclear whether this asymmetry is related to mass ejection, a steep gradient in the accretion rate, reaching some energetic limit in the disk, or some other unknown factors, but it is clear that there is significantly more to the behavior of the disk than the local Eddington process.

This brings us to the second puzzle: what causes the local Eddington effect to stop acting on the disk? In Neilsen et al. (2011), we found that in a double-peaked cycle, $R_{\rm in}$ grows at roughly constant temperature until $\phi \sim 0.9$, when the catastrophic changes take over to begin a new cycle in the disk. But for the single-peaked cycle shown in Figure 6, $R_{\rm in}$ stops growing and actually decreases slightly from $\phi \sim 0.75$–0.9. This momentary plateau in $R_{\rm in}$ signals the end of the local Eddington process, but here it occurs almost 10 s before the catastrophic changes in the disk. In other words, the plunge of $R_{\rm in}$ does not cause the end of the local Eddington effect (although they may coincide, as in double-peaked cycles; Neilsen et al. 2011). Instead, the end may be controlled by changes in the accretion rate. From our fits, this puzzling phase interval shows a steady $R_{\rm in}$ plus an increasing $T_{\rm obs}$, indicating an increasing accretion rate. So it may be that a particular range in $\dot{M}$ is required to maintain the local Eddington effect. But without a clear theoretical answer to these questions, we consider a number of intriguing possibilities for the disk evolution.

First, we can take the results of our phase-resolved spectroscopy at face value and use our disk parameters to infer the disk mass accretion rates for single- and double-peaked oscillations (Figure 7). We calculate the accretion rate using Equation (4) of Zimmerman et al. (2005). To facilitate a visual comparison, we also show the double-peaked $\dot{M}$ vertically normalized to match the mean value for the single-peaked cycle (green dashed line). The accretion rate is higher on average in the double-peaked cycle ($\dot{M} \approx 7.4 \times 10^{18}$ g s^{-1} versus $\dot{M} \approx 5.9 \times 10^{18}$ g s^{-1}), but the $\dot{M}$ wave is wider and has a smaller absolute amplitude. As an aside, this higher accretion rate implies a larger unstable region in the disk, which could explain why the cycle period is slightly larger for double-peaked cycles (e.g., Nayakshin et al. 2000). Considering the last seconds before/during the collapse of the disk, we see that $\dot{M}$ is sharply peaked in the single-peaked cycle, so that for a fixed phase-averaged accretion rate (i.e., comparing the normalized accretion rates), more matter accretes earlier in double-peaked oscillations.

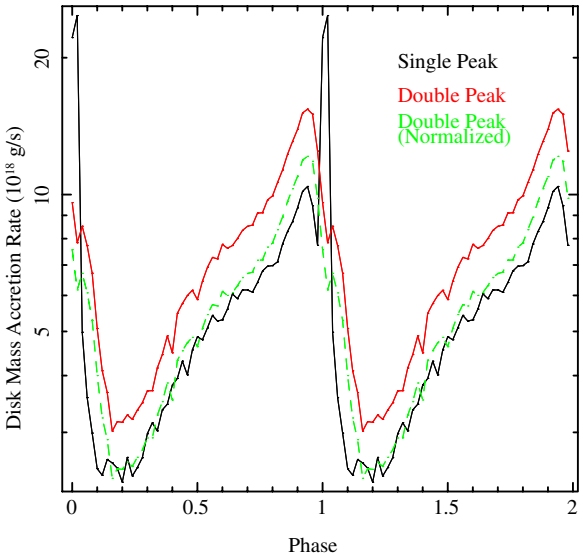

Figure 7. Accretion rates vs. phase implied by our fits to the phase-resolved PCA spectra of single- (black) and double-peaked heartbeats (red). For direct comparison, we also overplot $\dot{M}$ for the double-peaked cycle, normalized to the mean value for the single-peaked cycle (green dashed line). In double-peaked cycles, the accretion rate is higher and the wave of matter is sustained for longer; in single-peaked cycles, the overall accretion rate is lower and spikes sharply around $\phi = 0$. We discuss in Section 4 how the differences in the $\dot{M}$ profile may be responsible for the different X-ray light curves.

(A color version of this figure is available in the online journal.)

But this explanation is only valid to the extent that the accretion disk dominates both the mass flux and the X-ray emission. If there are outflows from very small radii[4] or if there is a second component, e.g., the corona, with a non-zero accretion rate or some difference radiative efficiency, then Figure 7 is only an approximation. We note that our accretion rates are calculated from the disk *prior to* Compton scattering. For this reason, the contribution of the corona could be further involved if there is significant mass transfer between it and the disk, as suggested by Janiuk & Czerny (2005) and verified by our fits here and in Neilsen et al. (2011). Janiuk & Czerny (2005) consider several different prescriptions for mass transfer between the accretion disk and the corona (i.e., dependent on the luminosity or the accretion rate in the disk). It could be that single- and double-peaked oscillations transfer mass differently, and that this controls the evolution of the local Eddington process in the disk. As the corona has a stabilizing effect on the disk (Janiuk & Czerny 2005), it may also be that the coronal geometry differs between different types of cycles, leading to different plunge behavior.

Figure 7 is also only accurate insofar as the disk can be approximated as having a constant radiative efficiency, optical depth, spectral hardening, and a constant/uniform accretion rate (in a given phase bin) in the inner disk. The accuracy of these approximations must be determined from simulations that calculate and fit spectra at each phase of the cycle and compare

[4] *Chandra* observations of GRS 1915+105 indicate the presence of winds, but these are typically driven from the outer disk (Miller et al. 2008; Neilsen & Lee 2009; Neilsen et al. 2011, 2012).

to the physical behavior of the accretion disk in the simulations. Since Nayakshin et al. (2000) and Janiuk & Czerny (2005) invoke strong variations in the disk viscosity and surface density, it may be that our approximations here are insufficient for a complete understanding of the evolution of the disk. On the other hand, it seems clear that the phase dependence of the accretion rate (whether as shown in Figure 7 or otherwise) is probably the primary factor in determining the strength and duration of the X-ray pulses, and may in some yet-to-be-determined way influence the duration of the local Eddington effect. Nayakshin et al. (2000) note that the cycle period and profile depend on the mass accretion rate in a nonlinear way, and it would be very interesting to see if future simulations including a local Eddington effect and mass transfer between the disk and corona (after Janiuk & Czerny 2005) could reproduce the peak structure of the observed cycles.

The need for future theoretical studies is also highlighted by a recent spectral study of a long *Beppo* SAX observation of the heartbeat state (Mineo et al. 2012). Dividing the cycles into five characteristic intervals, Mineo et al. (2012) followed the disk and corona during the cycle, and they observed behavior consistent with our present work and Neilsen et al. (2011): the disk radius increases at constant temperature and the coronal electron temperature drops when the disk plunges inward and the disk temperature spikes (i.e., in the hard pulse). However, their results suggested a *decrease* in the coronal optical depth during the hard pulse, which they interpreted as a condensation of the corona (in contrast to the sharp increase in the coronal optical depth reported here and in Neilsen et al. 2011 and interpreted as a result of mass ejection processes). Presently, it is unclear if this difference is due to their wider energy coverage ($\sim 4\times$), our superior phase resolution ($\sim 10\times$), or differences in our models, i.e., `simpl` versus `compPS` (which includes non-thermal electrons). But the similarities in our results are highly encouraging, and there is hope that new theoretical studies will allow us to converge on a complete understanding of the ρ state in the near future.

5. CONCLUSIONS

GRS 1915+105 exhibits a fascinating array of variability in its X-ray light curve. It is believed that many of its variability classes are related to limit cycles of accretion, advection, and ejection, but the origin of these variability classes is only understood to the degree that we understand their diversity. This is particularly true for the ρ state, which is similar to several other variability classes, and which displays striking variations from observation to observation, particularly with respect to the number of peaks per cycle in the X-ray light curve (e.g., Massaro et al. 2010; this work).

In a previous paper (Neilsen et al. 2011), we performed a detailed, phase-resolved spectral and timing study of GRS 1915+105 in a double-peaked instance of the ρ state. Building on our knowledge of this type of oscillation, we have presented here a comprehensive study of archival *RXTE* observations of the ρ-like cycles. Broadly, our results indicate that the variation in the heartbeat state light curves can be explained in the context of two main pulses, one soft and one hard, whose relative strengths, durations, and separations can vary smoothly over time. This explanation appears to apply whether each cycle exhibits one pulse, two pulses, or some intermediate morphology. Furthermore, phase-resolved spectra from the *RXTE* PCA clearly indicate that oscillations with very different profiles exhibit remarkably similar spectral evolution. We conclude that a common set of dominant accretion processes produces the diverse light curves.

In this context, what is particularly remarkable about the heartbeat state is the complex interaction between the disk, its mass accretion rate, and the radiation it produces. The oscillation is a process set in motion by a high external accretion rate, in which an unstable disk periodically sends waves of mass inward (e.g., Taam et al. 1997; Nayakshin et al. 2000; Janiuk & Czerny 2005). Responding to the increasing influx of matter, the disk produces enough radiation to slowly expel some fraction of the inflow, driving the inner edge of the disk away from the black hole. But eventually, the disk's ability to compensate is overwhelmed; when the accretion rate remains high, the excess matter in the inner disk plunges inward as the temperature and viscosity spike. But even in these final moments of the cycle, radiation pressure still manages to eject some mass from the disk. These are the common, interconnected processes that lead to the ρ-like cycles in GRS 1915+105.

But there is another process, the accretion disk wind, whose ubiquity has yet to be confirmed (see our upcoming *Chandra, RXTE, Gemini,* and *EVLA* study; J. Neilsen et al., in preparation). In Neilsen et al. (2011), we showed that the bright X-ray pulses from the inflow drive a massive, ionized wind off the outer disk ($R \lesssim 10^{11}$ cm). This wind can drain as much as 95% of the external mass supply from the accretion flow, suggesting that the companion star is actually supplying matter at a rate well in excess of Eddington (since matter reaches the black hole at roughly the Eddington rate). Massive winds have also been seen in other black holes (e.g., King et al. 2012; Ponti et al. 2012, and references therein) and neutron stars (e.g., GX 13+1; Ueda et al. 2004). Eventually, this massive wind depletes the outer disk, creating a mass deficit. The heartbeat oscillations continue unabated until, days or weeks later, this deficit propagates inward (Shields et al. 1986; Luketic et al. 2010; Neilsen et al. 2011), simultaneously suppressing the thermal–viscous instability, the local Eddington effect, radiation-pressure-driven mass ejection, and the accretion disk wind itself.

We end on an exciting note, for it is finally clear that GRS 1915+105 is not alone. In a new outburst detected by *Swift*/Burst Alert Telescope (Krimm et al. 2011) and followed up with frequent *RXTE* PCA observations, the black hole candidate IGR J17091–3624 was discovered to exhibit heartbeats and several other of GRS 1915+105's variability classes in its X-ray light curve (e.g., Pahari et al. 2011; Altamirano et al. 2011). But if GRS 1915+105's behavior is made possible by a high mass supply rate from its subgiant companion (Greiner et al. 2001), then is the presence of two active "GRS 1915+105"s in our Galaxy consistent with models of stellar and binary evolution? Thus, although at a much lower X-ray flux, future studies of IGR 17091–3624 will place strong constraints on the origin of accretion instabilities like those in GRS 1915+105.

We thank Diego Altamirano for provocative discussions of IGR 17091–3624 and GRS 1915+105. J.N. gratefully acknowledges funding support from Chandra grant G07-8044X and the Harvard University Graduate School of Arts and Sciences, as well as support from the National Aeronautics and Space Administration through the Smithsonian Astrophysical Observatory contract SV3-73016 to MIT for support of the *Chandra* X-ray Center, which is operated by the Smithsonian Astrophysical Observatory for and on behalf of the National Aeronautics Space Administration under contract NAS8-03060. R.A.R. acknowledges partial support from the NASA contract to MIT for

the support of *RXTE* instruments. This research has made use of data obtained from the High Energy Astrophysics Science Archive Research Center (HEASARC), provided by NASA's Goddard Space Flight Center.

REFERENCES

Altamirano, D., Belloni, T., Linares, M., et al. 2011, ApJ, 742, L17
Belloni, T., Klein-Wolt, M., Méndez, M., van der Klis, M., & van Paradijs, J. 2000, A&A, 355, 271
Belloni, T., Mendez, M., King, A. R., van der Klis, M., & van Paradijs, J. 1997, ApJ, 488, L109
Canizares, C. R., Davis, J. E., Dewey, D., et al. 2005, PASP, 117, 1144
Castro-Tirado, A. J., Brandt, S., & Lund, N. 1992, IAU Circ., 5590, 2
Dhawan, V., Mirabel, I. F., & Rodríguez, L. F. 2000, ApJ, 543, 373
Fender, R., & Belloni, T. 2004, ARA&A, 42, 317
Fender, R., Corbel, S., Tzioumis, T., et al. 1999, ApJ, 519, L165
Fender, R. P., Belloni, T. M., & Gallo, E. 2004, MNRAS, 355, 1105
Fukue, J. 2004, PASJ, 56, 569
Greiner, J., Cuby, J. G., & McCaughrean, M. J. 2001, Nature, 414, 522
Hannikainen, D. C., Rodriguez, J., Vilhu, O., et al. 2005, A&A, 435, 995
Heinzeller, D., & Duschl, W. J. 2007, MNRAS, 374, 1146
Houck, J. C. 2002, in High Resolution X-ray Spectroscopy with XMM-Newton and Chandra, ed. G. Branduardi-Raymont (London: MSSL)
Houck, J. C., & Denicola, L. A. 2000, in ASP Conf. Ser. 216, Astronomical Data Analysis Software and Systems IX, ed. N. Manset, C. Veillet, & D. Crabtree (San Francisco, CA: ASP), 591
Jahoda, K., Swank, J. H., Giles, A. B., et al. 1996, Proc. SPIE, 2808, 59
Janiuk, A., & Czerny, B. 2005, MNRAS, 356, 205
Janiuk, A., Czerny, B., & Siemiginowska, A. 2000, ApJ, 542, L33
King, A. L., Miller, J. M., Raymond, J., et al. 2012, ApJ, 746, L20
Klein-Wolt, M., Fender, R. P., Pooley, G. G., et al. 2002, MNRAS, 331, 745
Krimm, H. A., Barthelmy, S. D., Baumgartner, W., et al. 2011, ATel, 3144, 1
Lee, J. C., Reynolds, C. S., Remillard, R., et al. 2002, ApJ, 567, 1102
Lightman, A. P., & Eardley, D. M. 1974, ApJ, 187, L1
Lin, D., Remillard, R. A., & Homan, J. 2009, ApJ, 696, 1257
Luketic, S., Proga, D., Kallman, T. R., Raymond, J. C., & Miller, J. M. 2010, ApJ, 719, 515
Massaro, E., Ventura, G., Massa, F., et al. 2010, A&A, 513, A21
McClintock, J. E., Shafee, R., Narayan, R., et al. 2006, ApJ, 652, 518
Miller, J. M., Raymond, J., Reynolds, C. S., et al. 2008, ApJ, 680, 1359
Mineo, T., Massaro, E., D'Ai, A., et al. 2012, A&A, 537, A18
Mirabel, I. F., Dhawan, V., Chaty, S., et al. 1998, A&A, 330, L9
Mirabel, I. F., & Rodríguez, L. F. 1994, Nature, 371, 46
Nayakshin, S., Rappaport, S., & Melia, F. 2000, ApJ, 535, 798
Neilsen, J., & Lee, J. C. 2009, Nature, 458, 481
Neilsen, J., Petschek, A. J., & Lee, J. C. 2012, MNRAS, 421, 502
Neilsen, J., Remillard, R. A., & Lee, J. C. 2011, ApJ, 737, 69
Pahari, M., Yadav, J., & Bhattacharyya, S. 2011, arXiv:1105.4694
Paul, B., Agrawal, P. C., Rao, A. R., et al. 1998, ApJ, 492, L63
Ponti, G., Fender, R., Begelman, M., et al. 2012, MNRAS, in press (arXiv:1201.4172)
Shields, G. A., McKee, C. F., Lin, D. N. C., & Begelman, M. C. 1986, ApJ, 306, 90
Steiner, J. F., McClintock, J. E., Remillard, R. A., Narayan, R., & Gou, L. 2009, ApJ, 701, L83
Taam, R. E., Chen, X., & Swank, J. H. 1997, ApJ, 485, L83
Ueda, Y., Murakami, H., Yamaoka, K., Dotani, T., & Ebisawa, K. 2004, ApJ, 609, 325
Wilms, J., Allen, A., & McCray, R. 2000, ApJ, 542, 914
Yadav, J. S., Rao, A. R., Agrawal, P. C., et al. 1999, ApJ, 517, 935
Zdziarski, A. A., Johnson, W. N., & Magdziarz, P. 1996, MNRAS, 283, 193
Zimmerman, E. R., Narayan, R., McClintock, J. E., & Miller, J. M. 2005, ApJ, 618, 832
Życki, P. T., Done, C., & Smith, D. A. 1999, MNRAS, 309, 561